Modeling penny-shaped crack using a single high order smooth element

†*Hang Ma[1], Donghong He[2], and Zhao Guo[3]

[1]College of Sciences, Shanghai University, China
[2]Shanghai Institute of Applied Mathematics and Mechanics, Shanghai University, China
[3]College of Civil Engineering and Urban Construction, Jiujiang University, China

†*Presenting and corresponding author: hangma@shu.edu.cn

Abstract

A high order smooth element is constructed for modeling penny-shaped crack placed on but not limited to flat surface using a single element. The smoothness of the element is realized by repeated use of real nodes for interpolation in both the radial and circumferential directions of the element by taking advantage of geometrical features of the penny shape so that the end node/line effects existing in conventional low order elements have been removed. The technique of shape function manipulation is proposed to deal with the hyper-singular integrals in the boundary element method (BEM) for crack problems. The stress intensity factors under various loads are computed and compared with the analytical solutions in the numerical examples, showing the accuracy and effectiveness of the proposed high order smooth element.

Keywords: High order smooth element, Penny-shaped crack, Stress intensity factor, Hypersingular integral, Boundary element method

Introduction

In the three-dimensional fracture analysis of structures, penny-shaped cracks have long been one of the most investigated cracks since their good representativeness to the defects in the three-dimensional solids. Conventionally, the low-order elements are employed in the numerical fracture analysis [1]-[2]. In the case of analyzing fine details near crack tips [3] or multiple-cracks [4], huge numbers of elements have to be used, resulting in large solution scale of the problem, especially for the FEM. In addition, the hypersingular integrals have to be treated carefully in the use of boundary element method (BEM). Based on the Chebyshev polynomials, Chen proposed a Gauss type quadrature to evaluate the hypersingular integrals encountered over the whole flat crack [5], much like using a single element. Recently, Gao et al. proposed a series of isoparametric closure elements [6] and improved by Ma et al. to high order smooth elements [7] for modeling closed surfaces using a single element. In the present work, the high order smooth elements are extended for modeling penny-shaped crack on flat and spherical surfaces, combined with the proposed technique of shape function manipulation to deal with the hypersingular integrals in the BEM. The stress intensity factors (SIF) under various loads are computed and compared with the analytical solutions [8], showing the accuracy and effectiveness of the high order smooth element.

Construction of smooth element for crack

Crack discretization

Only the upper face of the penny-shaped crack needs to be discretized in the radial and circumferential directions. An example of the element with total nodes N=12 in the real and parametrical spaces are shown in Fig. 1a and 1b, respectively, where the symbols ○ and ◇ mean that the nodes are used repeatedly more than once in either circumferential or radial

directions for interpolations. The local intrinsic coordinates ξ_1 and ξ_2 correspond to the radial and circumferential lines. The double solid line Fig. 1b is the polar point of the element without placing node and the numbers with an apostrophe is for avoiding confusion of nodes which are used repeatedly. The digits in parentheses are the local counting numbers of nodes, which correlates with the global counting number, *m*, as follows

$$m = (k_1 - 1) \cdot N_2 + k_2 \,, \quad (k_1 = 1,..., N_1 \,; k_2 = 1,..., N_2) \tag{1}$$

where N_1 and N_2 represent the numbers of nodes on the radial and circumferential lines, and also the numbers of the circumferential and radial lines, respectively.

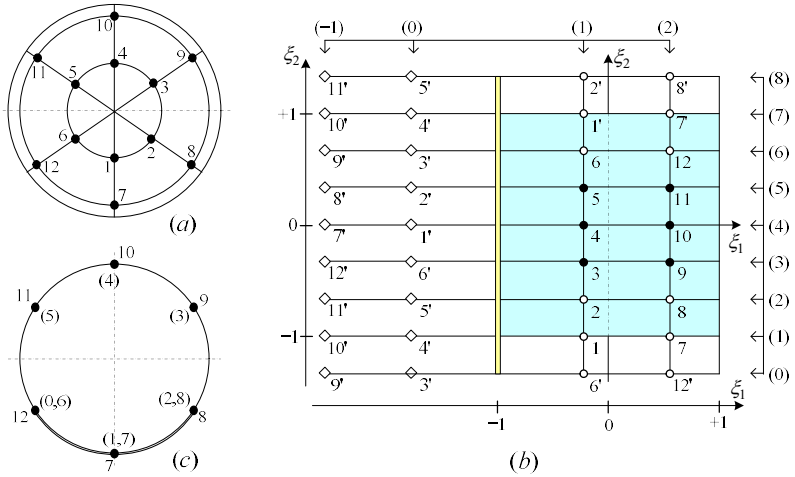

Figure 1. Crack discretization in real space (*a*), parametrical space (*b*) and along one of the circumferential lines (*c*)

Shape functions

The shape functions for the crack are formed by the product of the shape functions in both the circumferential and radial directions, just the same with the formation of closure elements [6]. However, the key idea for constructing smooth elements is the repeated use of nodes, with which the interpolation spans are expanded as shown in Fig. 1b. Along one of the circumferential lines as shown in Fig. 1c, three nodes with the global numbers 12, 7 and 8 are used twice. The digits in parentheses denote the local counting numbers from 0 to N_2+2, where the nodes used twice have two local counting numbers. The shape functions along circumferential lines are defined as follows

$$\phi_k^{(2)}(\xi) = l_k^{(N_2+2)}(\xi) + l_{N_2+k}^{(N_2+2)}(\xi), \quad (k = 1,2) \tag{2a}$$

$$\phi_k^{(2)}(\xi) = l_k^{(N_2+2)}(\xi), \qquad (k = 3,..., N_2 - 1) \tag{2b}$$

$$\phi_k^{(2)}(\xi) = l_0^{(N_2+2)}(\xi) + l_k^{(N_2+2)}(\xi), \quad (k = N_2) \tag{2c}$$

where $l_k^{(N_2+2)}$ represents the Lagrange interpolation polynomials of order N_2+2 as follows

$$l_k^{(N_2+2)}(\xi) = \prod_{j=0, j\neq k}^{N_2+2} \frac{(\xi - \xi_j)}{(\xi_k - \xi_j)}, \ (k = 0,1,..., N_2 + 2) \tag{3}$$

In radial directions, two auxiliary nodes denoted by ◇ as shown in Fig. 1b are supplemented across the pole so that the shape functions for crack surface are defined by

$$\phi_k^{(1)}(\xi) = l_k^{(N_1+1)}(\xi), \qquad (k = 1,..., N_1) \tag{4}$$

where $l_k^{(N_1+1)}$ represents also the Lagrange interpolation polynomials of order N_1+1 as follows

$$l_k^{(N_1+1)}(\xi)=\prod_{j=-1,j\neq k}^{N_1}\frac{(\xi-\xi_j)}{(\xi_k-\xi_j)},\quad (k=-1,0,...,N_1) \tag{5}$$

In this way, the shape functions for the crack surface can be obtained

$$\phi_m(\xi_1,\xi_2)=\phi_{k_1}^{(1)}(\xi_1)\cdot\phi_{k_2}^{(2)}(\xi_2),\quad (k_1=3,...,N_1) \tag{6a}$$

$$\phi_m(\xi_1,\xi_2)=\phi_{k_1}^{(1)}(\xi_1)\cdot\phi_{k_2}^{(2)}(\xi_2)+\phi_{1-k_1}^{(1)}(\xi_1)\cdot\phi_{M(k_2)}^{(2)}(\xi_2),\ (k_1=1,2) \tag{6b}$$

where $k_2=1,...,N_2$ and the counting numbers m, k_1 and k_2 in Eqs. (6a) and (6b) are correlated by Eq. (1). The subscript $M(k)$ is a mirror function about the pole defined as follows

$$M(k)=\begin{cases}k+N_2/2 & k\le N_2/2\\ k-N_2/2, & k>N_2/2\end{cases} \tag{7}$$

Thus in the construction of smooth element for cracks, the even number should be used for N_2. Although the variation spans of the two intrinsic variables ξ_1 and ξ_2 have been expanded, however, the integration spans for the smooth element remain still within [–1,+1], a shaded square region as shown in Fig. 1b. In consideration of the deformation feature of crack tip, the shape functions for the crack opening displacement (COD) take a different form as

$$\bar{\phi}_m(\xi_1,\xi_2)=\bar{\phi}_{k_1}^{(1)}(\xi_1)\cdot\phi_{k_2}^{(2)}(\xi_2),\quad (k_1=3,...,N_1) \tag{8a}$$

$$\bar{\phi}_m(\xi_1,\xi_2)=\bar{\phi}_{k_1}^{(1)}(\xi_1)\cdot\phi_{k_2}^{(2)}(\xi_2)+\bar{\phi}_{1-k_1}^{(1)}(\xi_1)\cdot\phi_{M(k_2)}^{(2)}(\xi_2),\ (k_1=1,2) \tag{8b}$$

where

$$\bar{\phi}_k^{(1)}(\xi)=\frac{\sqrt{1-\left[(1+\xi)/2\right]^2}}{\sqrt{1-\left[(1+\xi_k)/2\right]^2}}l_k^{(N_1+1)}(\xi),\qquad (k=1,...,N_1) \tag{9}$$

Therefore the smooth element for crack does not belong to the category of isoparametric elements. It need to be pointed out that the role of auxiliary nodes denoted by ◇ is nothing but to improve the fitting effect along radial lines, since the outward normal of the surface in the region indicated by ◇ turns upside-down from that of the shaded square region as shown in Fig. 1b. In addition, what needs to be emphasized is that the outward normal just at the pole is indeterminate since the circumferential line reduces to a single point at the pole. This is why no node be arranged at the pole for the crack element. It can be seen from the construction process that there is no end node and end line inside the smooth element. As a result, the interpolation accuracy of the smooth element will increase greatly with the removal of end node/line effects and the increase of the order of interpolation polynomials while the total number of nodes of the element is kept unchanged.

Dealing with singularities of integrals

Basic equations

The boundary integral equation (BIE) for a crack in full space is given below [9]

$$\tau_i(y)=-\mathrm{HFP}\int_A\delta_j(x)\tau_{ij}^C(x,y)\,dA(x),\quad y\in A \tag{10}$$

where A stands for the upper surface of the crack and τ_i the traction on A. x and y represent the field and source points, respectively. $\delta_j=u_j^+-u_j^-$ denotes the COD defined by the difference of displacements, u_j^+ and u_j^-, over the upper and lower surfaces of the crack. HFP means that the integral is evaluated in the Hadamard finite part sense. The kernel τ_{ij}^C is defined by

$$\tau_{ij}^C(x,y)=n_k(y)\tau_{ikj}^*(x,y) \tag{11}$$

In Eq. (11), n_k stands for the component of the outward normal and

$$\tau^*_{ijk}(x,y)=\frac{\mu}{4\pi(1-\nu)r^3}\left\{3\frac{\partial r}{\partial n}\left[(1-2\nu)\delta_{ij}r_{,k}+\nu\left(\delta_{ki}r_{,j}+\delta_{jk}r_{,i}\right)-5r_{,i}r_{,j}r_{,k}\right]\right.$$
$$\left.+3\nu\left(r_{,j}r_{,k}n_i+r_{,k}r_{,i}n_j\right)+(1-2\nu)\left(3r_{,i}r_{,j}n_k+\delta_{ki}n_j+\delta_{jk}n_i\right)-(1-4\nu)\delta_{ij}n_k\right\} \tag{12}$$

where μ and ν are the shear modulus and Poisson ratio of the material, respectively. r is the distance between the field and source points defined as

$$r=\sqrt{(x_k-y_k)(x_k-y_k)} \tag{13}$$

In a special case of a flat crack placed in the plane x_1-x_2 with only the normal load applied in x_3 direction, the expressions (10)-(12) can be written in much simplified forms [5][8]. However, in the present work, these forms are kept unchanged to cope with the general cases.

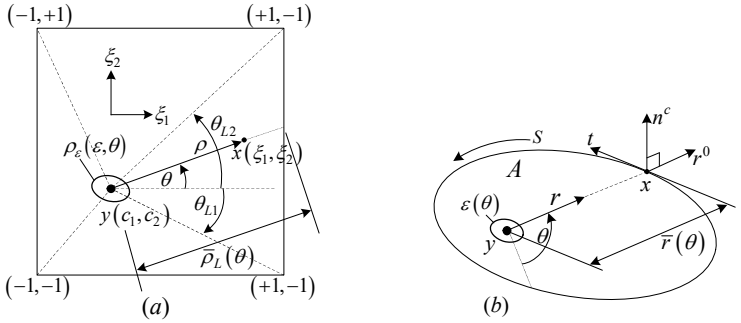

Figure 2. Domains for evaluating strong-singular (*a*) and hypersingular (*b*) integrals

Shape function manipulation and evaluation of strong-singular integral

Now rewrite Eq. (10) after discretizing the COD of the crack using the shape functions (8a) and (8b) as follows

$$\tau_i(y)=-\sum_{m=1}^{N}\delta_j^m I_{ij}^m \tag{14}$$

$$\delta_k(x)=\sum_{m=1}^{N}\delta_k^m\bar{\phi}^m\left[\xi_1(x),\xi_2(x)\right] \tag{15}$$

where

$$I_{ij}^m=\mathrm{HFP}\int_A\bar{\phi}^m\left[\xi_1(x),\xi_2(x)\right]\tau_{ij}^C(x,y)dA(x)$$
$$=\lim_{(\xi_1,\xi_2)\to(c_1,c_2)}\int_{-1}^{+1}\int_{-1}^{+1}\bar{\phi}^m(\xi_1,\xi_2)\tau_{ij}^C(\xi_1,\xi_2)J(\xi_1,\xi_2)d\xi_1 d\xi_2 \tag{16}$$

It needs to be pointed out that in Eq. (16) the upper crack surface A is discretized using the shape functions (6a) and (6b), different from that for the COD. The integrals (16) are to be evaluated in polar systems as shown in Fig. 2a as follows

$$I_{ij}^m=\lim_{\rho_\varepsilon\to 0}\sum_L\int_{\theta_{L1}}^{\theta_{L2}}\int_{\rho_\varepsilon}^{\bar{\rho}_L(\theta)}\bar{\phi}^m(\rho,\theta)\tau_{ij}^C(\rho,\theta)J(\rho,\theta)\rho d\rho d\theta \tag{17}$$

where (c_1,c_2) stand for the local coordinates of the source point y. Introduce the shape function manipulation as

$$\Delta\bar{\phi}^m=\bar{\phi}^m(\rho,\theta)-\bar{\phi}^m(c_1,c_2) \tag{18}$$

Rewrite integrals (17) as

$$I_{ij}^m=\lim_{\rho_\varepsilon\to 0}\sum_L\int_{\theta_{L1}}^{\theta_{L2}}\int_{\rho_\varepsilon}^{\bar{\rho}_L(\theta)}\Delta\bar{\phi}^m\tau_{ij}^C(\rho,\theta)J(\rho,\theta)\rho d\rho d\theta+\bar{\phi}^m(c)\lim_{\rho_\varepsilon\to 0}\sum_L\int_{\theta_{L1}}^{\theta_{L2}}\int_{\rho_\varepsilon}^{\bar{\rho}_L(\theta)}\tau_{ij}^C(\rho,\theta)J(\rho,\theta)\rho d\rho d\theta$$

$$= I_{ij\text{CPV}}^{m} + \bar{\phi}_m(c_1,c_2)\lim_{x\to y}\int_A \tau_{ij}^{C}(x,y)\,dA(x) = I_{ij}^{m\text{CPV}} + \bar{\phi}^m(c_1,c_2)\,I_{ij}^{\text{HFP}} \tag{19}$$

by subtracting then adding back a shape function at the singular source point. It is seen that the first integral $I_{ij}^{m\text{CPV}}$ at the right hand side of Eq. (19) is reduced to strong-singular integrals to be evaluated in the sense of Cauchy principal value (CPV). Expand the integrand of $I_{ij}^{m\text{CPV}}$ in (19) in truncated Laurent expansion at a fixed angle θ as follows

$$\tau_{ij}^{C}(\rho,\theta)\Delta\bar{\phi}^m J(\rho,\theta)\rho = \frac{1}{\rho}\tau_{ij}^{0}(\rho,\theta)\frac{\Delta\bar{\phi}^m}{\rho}J(\rho,\theta)\left(\frac{r}{\rho}\right)^{-3} = \frac{A_{ij}^{m}(\theta)}{\rho} + O(1) \tag{20}$$

where

$$\tau_{ij}^{0}(x,y) = r^3\tau_{ij}^{C}(x,y) \tag{21}$$

$$A_{ij}^{m}(\theta) = \lim_{\rho\to 0}\tau_{ij}^{0}(\rho,\theta)\frac{\Delta\bar{\phi}^m}{\rho}J(\rho,\theta)\left(\frac{r}{\rho}\right)^{-3} = \tau_{ij}^{0}(\theta)\bar{\phi}_{\rho}^{m}(\theta)J^{-2}(\theta) \tag{22}$$

$$\bar{\phi}_{\rho}^{m}(\theta) = \lim_{\rho\to 0}\frac{\Delta\bar{\phi}^m}{\rho} = \left[\frac{\partial\bar{\phi}^m}{\partial\xi_1}\cos\theta + \frac{\partial\bar{\phi}^m}{\partial\xi_2}\sin\theta\right]_{\rho=0} \tag{23}$$

In this way, the strong-singular integrals $I_{ij}^{m\text{CPV}}$ can be evaluated using the conventional Gauss quadrature in the following form

$$\begin{aligned} I_{ij}^{m\text{CPV}} &= \sum_L \int_{\theta_{L1}}^{\theta_{L2}} \left\{ \int_0^{\bar{\rho}_L(\theta)} \left[\Delta\bar{\phi}^m\tau_{ij}^{C}(\rho,\theta)J(\rho,\theta)\rho - \frac{A_{ij}^{m}(\theta)}{\rho}\right]d\rho + A_{ij}^{m}(\theta)\lim_{\rho_\varepsilon\to 0}\int_{\rho_\varepsilon}^{\bar{\rho}_L(\theta)}\frac{d\rho}{\rho}\right\}d\theta \\ &= \sum_L \int_{\theta_{L1}}^{\theta_{L2}}\int_0^{\bar{\rho}_L(\theta)}\left[\Delta\bar{\phi}^m\tau_{ij}^{C}(\rho,\theta)J(\rho,\theta)\rho - \frac{A_{ij}^{m}(\theta)}{\rho}\right]d\rho d\theta + \int_0^{2\pi} A_{ij}^{m}(\theta)\ln\left[\bar{\rho}_L(\theta)J_0(\theta)\right]d\theta \end{aligned} \tag{24}$$

Evaluation of hypersingular integral

The second integrals I_{ij}^{HFP} at the right hand side of Eq. (19) have no shape function, resulted from the shape function manipulation stated previously. Noticed that the kernels appeared in these integrals describe a divergence-free field [10], having the properties of

$$\lim_{x\to y}\oint_\Gamma \tau_{ij}^{C}(x,y)\,d\Gamma(x) = 0 \tag{25}$$

over a closed surface, suggesting that the integrals I_{ij}^{HFP} are surface independent, which can be and should be made use of. As shown in Fig. 2b, when the point *x* move along the boundary *S* of the crack, the straight line connecting *x* and *y*, or the generatrix, will form a new surface, over which the evaluation of integrals I_{ij}^{HFP} can be carried out instead of the original crack surface *A*. The shape of the new surface would be planar or conical, depending on whether the original crack is a flat or curved surface. In either of the cases, however, the component of the kernel τ_{ij}^{C} on the generatrix is constant at a fixed angle θ because n^c $\left(\vec{n}^c = \vec{r}^{\,0}\times\vec{t}\right)$ and $r_{,k}$ are all constants on the generatrix, where n^c is the outward normal of the new surface, r^0 the unit vector in *r* direction. See Fig. 2b and Eqs. (11)-(12). Therefore

$$\begin{aligned} I_{ij}^{\text{HFP}} &= \lim_{x\to y}\int_A \tau_{ij}^{C}(x,y)\,dA(x) = \lim_{\varepsilon\to 0}\int_0^{\alpha}\int_{\varepsilon}^{\bar{r}(\theta)} r^{-3}\tau_{ij}^{0}(\theta)\,r\,dr\,d\theta \\ &= -\int_0^{\alpha}\bar{r}^{-1}(\theta)\tau_{ij}^{0}(\theta)\,d\theta + \lim_{\varepsilon\to 0}\int_0^{\alpha}\varepsilon^{-1}(\theta)\tau_{ij}^{0}(\theta)\,d\theta \end{aligned} \tag{26}$$

where α is the solid angle of the cone surface and in particular $\alpha = 2\pi$ for planar surface. For a physical problem, the integral above should exist, which means that the infinite term or the last term at the right hand side of Eq. (26) should be eliminated or should be cancelled out by free terms [11]. Finally, the integrals I_{ij}^{HFP} can be evaluated using the conventional Gauss quadrature in the following form

$$I_{ij}^{\mathrm{HFP}} = -\oint_S \bar{r}^{-2}(x)\,\tau_{ij}^{0}(x,y)\,dS(x) \tag{27}$$

Numerical examples

Computation of SIF

In the numerical examples, the SIFs, K_1, K_2 and K_3 are computed by the corresponding COD values, δ^n, δ^b and δ^t in the open, shear and tear modes, respectively, at the point x in the local coordinate system $\left(\vec{b}=\vec{t}\times\vec{n}\right)$ as shown in Fig. 3a using the following approximate equations

$$K_1 = \frac{E}{4\left(1-\nu^2\right)}\sqrt{\frac{\pi}{2\Delta}}\delta^n \;,\; K_2 = \frac{E}{4\left(1-\nu^2\right)}\sqrt{\frac{\pi}{2\Delta}}\delta^b \;,\; K_3 = \frac{E}{4\left(1-\nu^2\right)}\sqrt{\frac{\pi}{2\Delta}}\delta^t \tag{28}$$

where Δ represents a small distance from the point x to the crack front and E is Young's modulus of the material. In the situation that the crack surfaces are traction free in full space under far-field loads, the computation model needs to be decomposed into two parts in the numerical analysis of such cracks. In the first part of the model, the tractions equal and opposite to the applied loads are acting on the crack surfaces without the far-field loads. In the second part of the model, the full space is loaded by the far-field loads without cracks. The final response is the linear superposition of the two parts of the model. However, the second part has no direct contribution to the values of SIF.

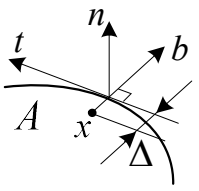

(*a*)

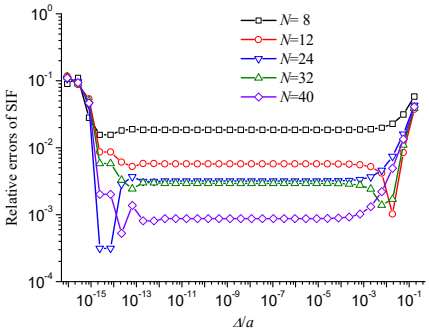

(*b*)

Figure 3. Local coordinate system (*a*) and errors of computed SIF as function of Δ (*b*)

Suitable distance check

Firstly, the suitable distance Δ is checked by a penny-shaped crack of radius a placed in the plane x_1-x_2 (x_3=0) in full space under a far-field unit normal load in x_3 direction, discretized using a single smooth element with a series of total node numbers from N=8 to N=40. The relative errors of computed SIF are depicted in Fig. 3b as a function of Δ, showing that the accuracy is satisfactory with such few nodes using a single smooth element. The results are fairly stable in a wide range of Δ so that Δ/a=10^{-4} is adopted in the following examples.

SIF under various normal loads

Secondly, the SIFs of the penny-shaped crack in full space under various far-field normal loads are computed using a single smooth element with the total node number N=32 and compared with the analytical solutions [8]. The normal loads are expressed by

$$\sigma_0 = c_0 + c_1\frac{x_1}{a} + c_2\frac{x_2}{a} + c_3\frac{x_1x_2}{a^2} + c_4\left(\frac{x_1}{a}\right)^2 + c_5\left(\frac{x_2}{a}\right)^2 \tag{29}$$

The coefficients for the 4 kinds of loads are listed in Table 1. The SIFs along the crack front are computed and shown in Fig. 4a while the angle θ is starting from the positive direction of x_1. It is seen from Fig. 4a that the computed results are in good agreement with those of analytical solutions, showing the accuracy and effectiveness of the proposed high order smooth element for the crack.

Table 1. Coefficients in Eq. (29)

Load	c_0	c_1	c_2	c_3	c_4	c_5
1	1	-1	-1	0	0	0
2	1	-1	0	0	0	0
3	1	0	0	-1	0	0
4	1	0.8	-0.9	0.5	0.08	0.02

SIF under unit shear load

Next example considers the penny-shaped crack in full space under far-field unit shear load in x_1 direction using a single smooth element with the total node number N=32. It is seen from Fig. 4b that the computed SIF in shear and tear modes (K_2 and K_3) varies along the crack front while the SIF in open mode (K_1) keeps zero throughout as expected.

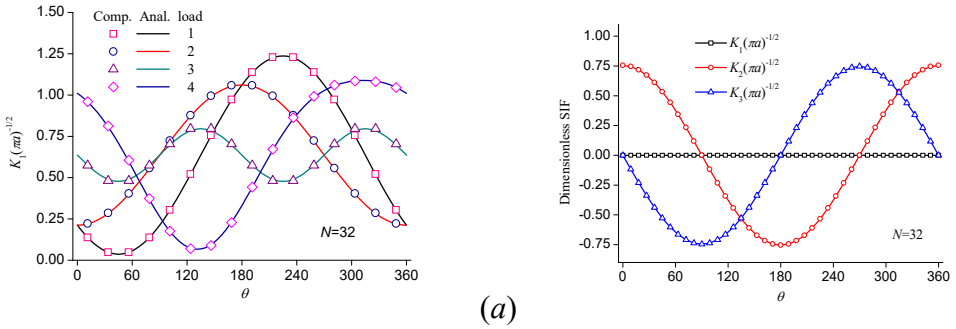

(*a*) (*b*)

Figure 4. Comparison of computed SIF under various far-field normal loads (*a*) and computed SIF under far-field unit shear load (*b*)

SIF of cracks on spherical surface

In the last example, the curved penny-shaped cracks on a spherical surface of radius R are computed under far-field unit normal load as shown in Fig. 5a using a single smooth element with the total node number N=40. The computed SIFs are presented in Fig. 5b with R/a, where the shape of the crack becomes a half-sphere when R/a=1 but behave towards a flat crack when R/a is very large. It is shown from Fig. 5b that that the SIF in open and shear modes (K_1 and K_2) increase gradually with R/a while the SIF in tear mode (K_3) keeps zero throughout as expected.

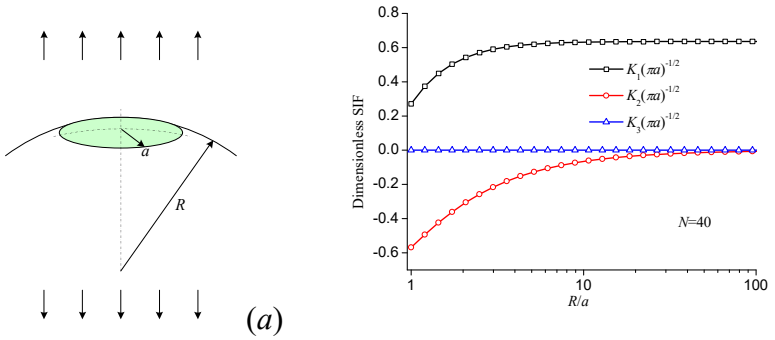

(*a*) (*b*)

Figure 5. Curved penny-shaped cracks on a spherical surface (*a*) with computed SIF (*b*) under far-field unit normal load

Conclusions

In the present work, a high order smooth element is constructed successfully for modeling penny-shaped crack placed on flat or curved surface using a single element. By making full use of geometrical features such as the symmetry and periodicity, the smoothness of the element is realized by repeated use of nodes in the radial and circumferential lines for interpolation. As a result, the accuracy of the crack modeling increases because of the raise of the order of interpolation polynomials as well as the removal of the end node/line effects existing in conventional low order elements. The technique of shape function manipulation is proposed to deal with the hyper-singular integrals in the BEM for crack problems. In the numerical examples, the accuracy and effectiveness of the proposed high order smooth element and the technique for hyper-singular integrals are verified by the computed SIFs, using a single element with such few nodes, compared with the analytical solutions.

Acknowledgement: The support of the present work by National Natural Science Foundation of China (Nos.11672173, 11272195, 11662005) is acknowledged.

References

[1] Cruse, T.A. (1988) *Boundary Element Analysis in Computational Fracture Mechanics*, Kluwer Academic Publishers, Dordrecht, Netherlands.

[2] Aliabadi, M.H. and Rooke, D.P. (1991) *Numerical Fracture Mechanics*, Computational Mechanics Publications, Southampton, UK.

[3] Wang, X. (2004) Elastic T-stress solutions for penny-shaped cracks under tension and bending, *Engineering Fracture Mechanics* **71**, 2283–2298.

[4] Tsang, D.K.L., Oyadiji, S.O. and Leung, A.Y.T. (2004) Multiple penny-shaped cracks interaction in a finite body and their effect on stress intensity factor, *Engineering Fracture Mechanics* **70**, 2199–2214.

[5] Chen, Y.Z. and Lee, K.Y. (2001) Numerical solution of three-dimensional crack problem by using hypersingular equation, *Computer Methods in Applied Mechanics and Engineering* **190**, 4019–4026.

[6] Gao, X.W., Yuan, Z.C., Peng, H.F., Cui. M. and Yang, K. (2016) Isoparametric closure elements in boundary element method, *Computers and Structures* **168**, 1–15.

[7] Ma, H., Tian, Y. and He, D.H. (2019) High order isoparametric elements in boundary element method—smooth elliptical element, *Engineering Analysis with Boundary Elements* **101**, 34–47.

[8] Atroshchenko, E., Potapenko, S. and Glinka, G. (2009) Stress intensity factor for an embedded elliptical crack under arbitrary normal loading, *International Journal of Fatigue* **31**, 1907–1910.

[9] Telles, J.C.F., Castor, G.S. and Guimaraes, S. (1995) A numerical Green's function approach for boundary elements applied to fracture mechanics, *International Journal for Numerical Methods in Engineering* **38**, 3259–3274.

[10] Ma, H. and Kamiya, N. (2002) A general algorithm for the numerical evaluation of nearly singular boundary integrals of various orders for two- and three-dimensional elasticity, *Computational Mechanics* **29**, 277–288.

[11] Gao, X.W. (2010) An effective method for numerical evaluation of general 2D and 3D high order singular boundary integrals, *Computer Methods in Applied Mechanics and Engineering* **199**, 2856–2864.